

THE TRANSIT LIGHT CURVE PROJECT. XIV. CONFIRMATION OF ANOMALOUS RADII FOR THE EXOPLANETS TRÉS-4b, HAT-P-3b, AND WASP-12b

TUCKER CHAN¹, MIKAEL INGEMYR^{1,2,3}, JOSHUA N. WINN¹, MATTHEW J. HOLMAN⁴,
ROBERTO SANCHIS-OJEDA¹, GIL ESQUERDO⁴, MARK EVERETT⁵

Draft version September 10, 2018

ABSTRACT

We present transit photometry of three exoplanets, TrES-4b, HAT-P-3b, and WASP-12b, allowing for refined estimates of the systems' parameters. TrES-4b and WASP-12b were confirmed to be “bloated” planets, with radii of $1.706 \pm 0.056 R_{\text{Jup}}$ and $1.736 \pm 0.092 R_{\text{Jup}}$, respectively. These planets are too large to be explained with standard models of gas giant planets. In contrast, HAT-P-3b has a radius of $0.827 \pm 0.055 R_{\text{Jup}}$, smaller than a pure hydrogen-helium planet and indicative of a highly metal-enriched composition. Analyses of the transit timings revealed no significant departures from strict periodicity. For TrES-4, our relatively recent observations allow for improvement in the orbital ephemerides, which is useful for planning future observations.

1. INTRODUCTION

A puzzling feature of the hot Jupiters is that many of them have radii that are either larger or smaller than one would have guessed prior to the discovery of this class of objects. This “radius anomaly problem” has been present since the first transiting planet was discovered by Charbonneau et al. (2000) and Henry et al. (2000), and still has no universally acknowledged resolution. Fortney & Nettelmann (2010) have reviewed many of the proposed solutions, and even in the short time since their review several other theories have been proposed (see, e.g., Perna et al. 2010; Batygin & Stevenson 2010). The small size of some planets can be explained as a consequence of heavy-metal enrichment, beyond the enrichment factors of Jupiter and Saturn and comparable to those of Uranus and Neptune. As for the larger radii, possible explanations include tidal friction, unexpected atmospheric properties, and resistive heating from electrical currents driven by star-planet interactions.

This paper presents follow-up observations of three exoplanets that were found to have anomalous radii. As in previous papers in this series, the purpose of the observations was to refine the system parameters (thereby checking on the magnitude of the radius problem) and to check for any transit timing anomalies that might be caused by additional gravitating bodies in the system.

Two of our targets are among the most “bloated” planets known. TrES-4 was discovered by Mandushev et al. (2007), and the two high-precision light curves that accompanied the discovery paper were reanalyzed by Torres et al. (2008) and Sozzetti et al. (2009). Here, we present 5 new light curves for this system. We also present 2 new light curves for WASP-12, a planet that was discovered by Hebb et al. (2009) and for which occultation photometry has been used to

characterize the planet's atmosphere and orbit (Campo et al. 2010; Madhusudhan et al. 2011). Our third target, HAT-P-3 (Torres et al. 2007), is in the opposite category of planets that are “too small.” Gibson et al. (2010) have published 7 high-quality light curves of the system. We present six new light curves, and provide independent estimates of the planetary and stellar parameters.

2. OBSERVATIONS AND DATA REDUCTION

Almost all the observations were conducted at the Fred Lawrence Whipple Observatory (FLWO) located on Mt. Hopkins, Arizona, using the 1.2m telescope and KeplerCam detector. The KeplerCam is a 4096² CCD with a field of view of 23'1 × 23'1. The pixels were binned 2 × 2 on the chip for faster readout. The binned pixels subtend 0'68 on a side. Observations were made through Sloan *i* and *z* filters. One of the WASP-12 transits was observed with the Nordic Optical Telescope (NOT) located in the Canary Islands, using the ALFOSC detector. The ALFOSC detector is a 2048² CCD with a field of view of 6'4 × 6'4, corresponding to 0'19 per pixel. The observation was made through a Johnson *V* filter. On each night we attempted to observe the entire transit, with at least an hour before ingress and an hour after egress, but the weather did not always cooperate.

We performed overscan correction, trimming, bias subtraction and flat-field division with IRAF⁶. To generate the light curves, we performed aperture photometry on the target star and all the comparison stars with similar brightnesses to the target star (within about a factor of two). We tried many different choices for the photometric aperture and found, unsurprisingly, that the best aperture diameter was approximately twice the full width at half maximum (FWHM) of the star. A comparison signal was formed from the weighted average of the flux histories of the comparison stars. The weights were chosen to minimize the out-of-transit (OOT) noise level. Some comparison stars that did not seem to provide a good correction were rejected. In general, 6-8 comparison stars were used to generate the final comparison signal. The target star's flux history was divided by the comparison signal

⁶ IRAF is distributed by the National Optical Astronomy Observatory, which is operated by the Association of Universities for Research in Astronomy (AURA) under cooperative agreement with the National Science Foundation.

¹ Department of Physics, and Kavli Institute for Astrophysics and Space Research, Massachusetts Institute of Technology, Cambridge, MA 02139, USA

² Research Science Institute, Center for Excellence in Education, 8201 Greensboro Drive, Suite 215, McLean, VA 22102, USA

³ Present address: Sillegårdsgatan 12, 686 95, Värtra Ämtervik, Sweden

⁴ Harvard-Smithsonian Center for Astrophysics, 60 Garden Street, Cambridge, MA 02138, USA

⁵ Planetary Science Institute, 1700 E. Fort Lowell Rd., Suite 106, Tucson, AZ 85719

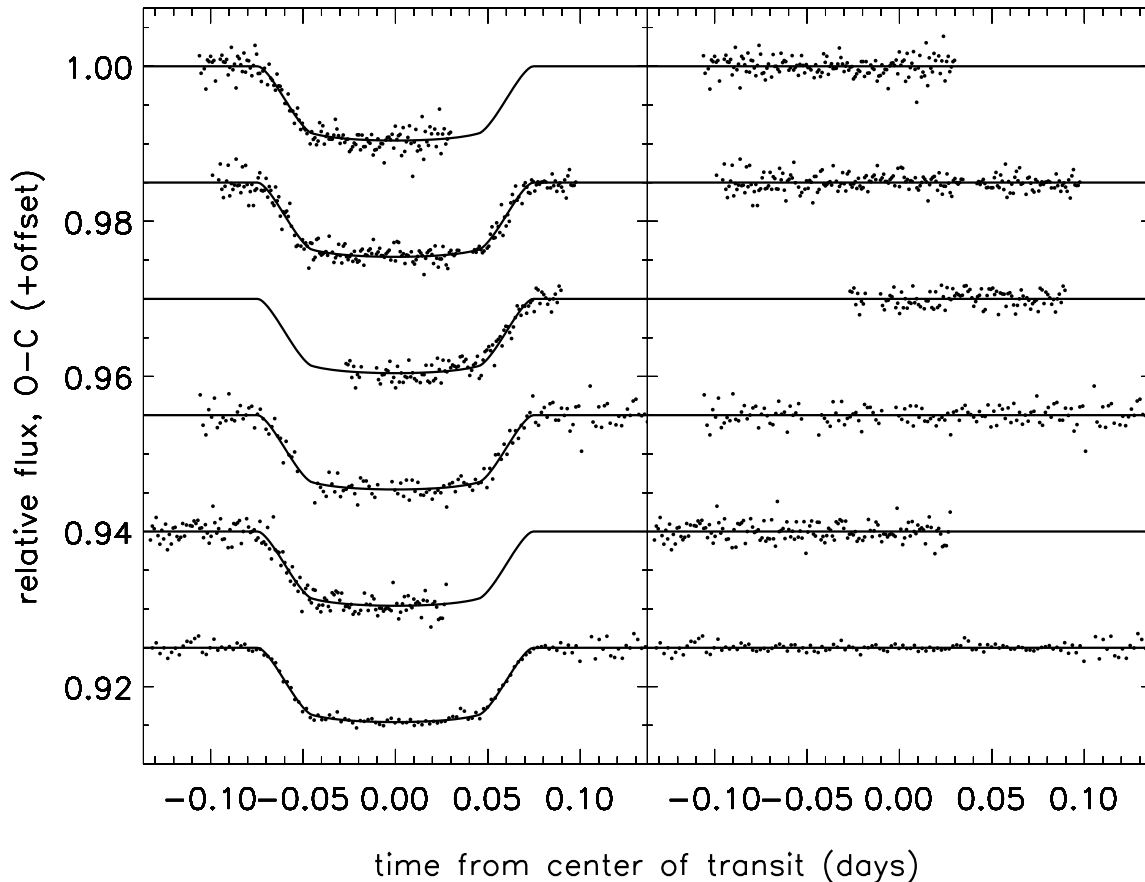


FIG. 1.— Relative photometry of TrES-4 in the i -band. From top to bottom, the observing dates are 2008 Jun 10, 2009 Apr 1, 2009 May 3, 2010 Apr 27 and 2010 May 4. See Table 1 for the cadence and rms residual of each light curve. The bottom plot is a composite light curve averaged into 3 min bins.

and then multiplied by a constant to give a mean flux of unity outside of the transit.

Table 1 is a journal of all our observations, including those that were spoiled by bad weather. The light curves are displayed in Figures 1–4, after having been corrected for differential extinction. Section 3 explains how this correction was applied. The airmass-corrected data are given in electronic form in Tables 2-4.

3. DETERMINATION OF SYSTEM PARAMETERS

Our techniques for light-curve modeling and parameter estimation are similar to those employed in previous papers in this series (see, e.g., Holman et al. 2006; Winn et al. 2007a). The basis for the light-curve model was the formula of Mandel & Agol (2002), assuming quadratic limb darkening and a circular orbit. The set of model parameters included the planet-to-star radius ratio (R_p/R_*), the stellar radius in units of orbital distance (R_*/a), the impact parameter ($b \equiv a \cos i / R_*$, where i is the orbital inclination), the time of conjunction for each individual transit (T_c), and the limb-darkening parameters u_1 and u_2 . We also fitted for two parameters (Δm_0 , k_z) specifying a correction for differential extinction,

$$\Delta m_{\text{cor}} = \Delta m_{\text{obs}} + \Delta m_0 + k_z z, \quad (1)$$

where z is the airmass, Δm_{obs} is the observed magnitude, and Δm_{cor} is the corrected magnitude that to be compared to the idealized transit model.

Since the data are not precise enough to determine both of the limb-darkening parameters, we followed the suggestion of Pál (2008) to form uncorrelated linear combinations of those parameters. We allowed the well-constrained combination to be a free parameter and held the poorly-constrained combination fixed at a tabulated value for a star of the appropriate type. In Pál’s notation, the rotation angle ϕ was taken to be near 37° in all cases. To determine the tabulated values we used a program kindly provided by J. Southworth to query and interpolate the tables of Claret (2004).⁷

For parameter estimation, we used a Markov Chain Monte Carlo (MCMC) algorithm to sample from the posterior probability distribution, employing the Metropolis-Hastings jump criterion and Gibbs sampling. Uniform priors were adopted for all parameters, and the likelihood was taken to be $\exp(-\chi^2/2)$ with

$$\chi^2 = \sum_{i,j} \left(\frac{f_{\text{obs},i,j} - f_{\text{calc},i,j}}{\sigma_{i,j}} \right)^2 \quad (2)$$

⁷ The interpolated values (u_1, u_2) for the cases of TrES-4 i , HAT-P-3 i , HAT-P-3 z , WASP-12 z , and WASP-12 V are (0.20, 0.37), (0.38, 0.27), (0.30, 0.29), (0.14, 0.36), (0.36, 0.35), respectively.

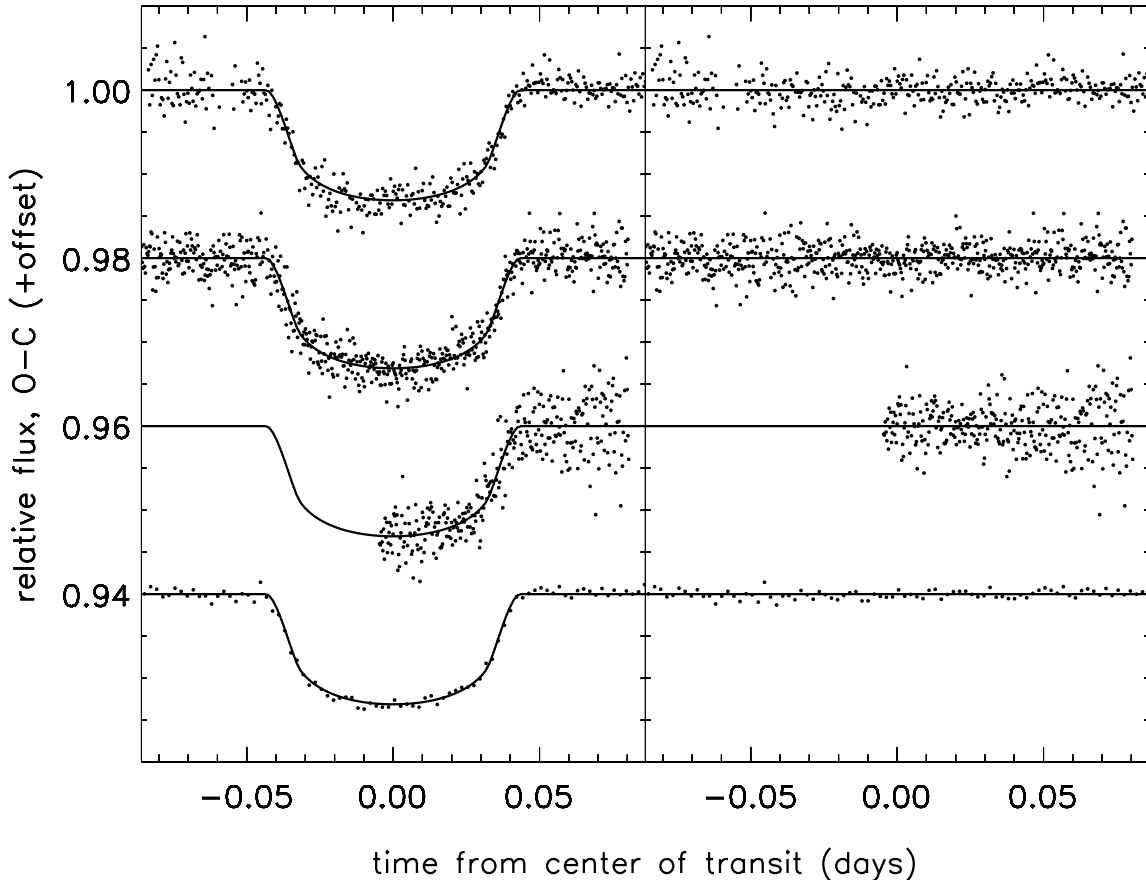


FIG. 2.— Relative photometry of HAT-P-3 in the i -band. From top to bottom, the observing dates are 2008 Mar 8, 2008 Apr 6 and 2008 May 5. See Table 1 for the cadence and rms residual of each light curve. The bottom plot is a composite light curve averaged into 3 min bins.

where $f_{\text{obs},i,j}$ is the j th data point from the i th light curve, $f_{\text{calc},i,j}$ is the calculated light curve based on the current parameters, and $\sigma_{i,j}$ is the uncertainty associated with $f_{\text{obs},i,j}$. All the light curves for a given planet were fitted simultaneously. The uncertainties were determined in a two-step process. First, the standard deviation σ_i of the OOT data was determined for each light curve. In a few cases, the pre-transit and post-transit noise levels were very different (due to different airmasses); in these cases the starting point was a function $\sigma_{i,j}$ that interpolated linearly between the two differing noise levels. Second, the preceding uncertainty estimates were multiplied by a correction factor $\beta \geq 1$ intended to account for time-correlated noise. The β factor was determined with the “time-averaging” procedure (Pont et al. 2006; Winn et al. 2008; Carter & Winn 2009), using bin sizes bracketing the ingress/egress duration by a factor of 2. The values of β are given in Table 1.

The starting point for each Markov chain was determined by minimizing χ^2 , and then perturbing those parameters by Gaussian random numbers with a standard deviation of 10σ , where σ is the rough uncertainty estimate returned by the least-squares fit. We ran several test chains to establish the appropriate jump sizes, giving acceptance rates near 40%. Then we ran 4–5 chains each with 10^6 links, ignored the initial 20% of each chain, and ensured convergence according to the

Gelman-Rubin statistic (Gelman & Rubin 1992). The quoted value for each parameter is the median of the one-dimensional marginalized posterior, and the quoted uncertainty interval encloses 68.3% of the probability (ranging from the 15.85% to the 84.15% levels of the cumulative probability distribution).

4. RESULTS

The results for the model parameters, and various derived parameters of interest, are given in Tables 5, 6 and 7. The next subsection explains how the stellar and planetary dimensions were calculated from the combination of light-curve parameters and stellar-evolutionary models. This is followed by a subsection presenting an examination of the transit times.

4.1. The stellar and planetary radii

The stellar and planetary radii and masses cannot be determined from transit parameters alone. The route we followed to determining these dimensions was to set the mass scale by using an estimated stellar mass M_* and the observed semi-amplitude K_* of the star’s radial-velocity orbit. The stellar mass is itself estimated by using stellar-evolutionary models with inputs from the observed spectral parameters, as well as the mean density that is calculated from the light-curve parameters. For the relevant formulas and discussion see Sozzetti et al. (2007) or Winn (2010). We used previously measured values of K_* , documented in Tables 5, 6 and 7.

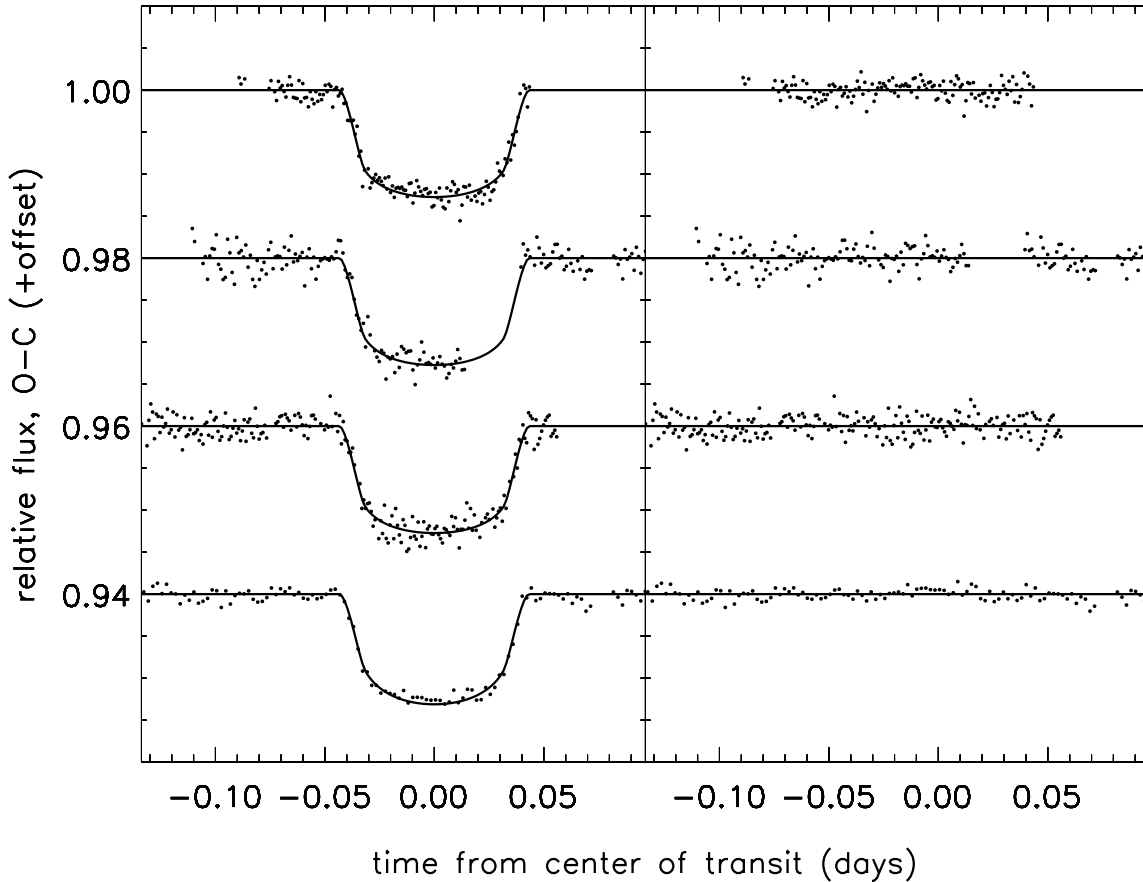


FIG. 3.— Relative photometry of HAT-P-3 in the z -band. From top to bottom, the observing dates are 2009 Mar 14, 2009 Mar 20 and 2009 Apr 15. See Table 1 for the cadence and rms residual of each light curve. The bottom plot is a composite light curve averaged into 3 min bins.

For the evolutionary models, we used the Yonsei-Yale (Y^2) isochrones (Yi et al. 2001).

The Y^2 isochrones can be thought of as an algorithm that takes as input the age, metallicity, mass, and concentration of α -elements of a star, and returns the star’s temperature, mass, density, and other properties. We interpolated the Y^2 isochrones in age from 0.1 to 14 Gyr in steps of 0.1 Gyr, and in metallicity from -0.20 to 0.58 dex in steps of 0.02 dex. Then we used linear interpolation to create a $4 \times$ finer mass sampling for each metallicity and age. We assumed the concentration of α -elements to be solar. To each model star in the resulting Y^2 grid, we assigned a likelihood based on the measured metallicity Z and effective temperature T_{eff} (taken from the literature) as well as the stellar mean density ρ_* determined solely from the transit parameters. Following Carter et al. (2009), the likelihood was taken to be proportional to $n \exp(-\chi^2/2)$, where

$$\chi^2 = \left(\frac{Z - Z_{\text{obs}}}{\sigma_Z} \right)^2 + \left(\frac{T_{\text{eff}} - T_{\text{eff,obs}}}{\sigma_{T_{\text{eff}}}} \right)^2 + \left(\frac{\rho_*}{\rho_{*,\text{obs}}} \right)^2, \quad (3)$$

and n is the number density of stars as a function of mass, according to Salpeter’s law with exponent -1.35 . The effect of multiplying by n is to set a prior so that extremely rare and short-lived stars are disfavored, even though they might provide a good fit. (The effect of this prior was generally small.)

Finally, the “best-fitting” values and uncertainties were computed from the appropriate likelihood-weighted integrals in the space of model stars.

With the stellar mass thereby determined, it is possible to compute the other dimensions R_p , R_* , and M_p . The results are given in Tables 5, 6 and 7. We note that this procedure does not take into account any uncertainty in the Y^2 isochrones themselves and, therefore, is subject to systematic errors that probably amount to a few percent (see, e.g., Torres et al. 2008).

4.2. Transit times and revised ephemerides

We analyzed the new transit times in conjunction with previously published midtransit times, to seek evidence for significant discrepancies from strict periodicity and refine the ephemerides to allow for accurate prediction of future events. The new transit times are given in Tables 8, 9 and 10, with uncertainties determined by the MCMC analysis described in Section 3. Previously published midtransit times were taken from Gibson et al. (2010), Hebb et al. (2009), Sozzetti et al. (2009), Torres et al. (2007), and Mandushev et al. (2007).

The transit times for each system were fitted with a linear function,

$$T_C = T_0 + E \cdot P \quad (4)$$

where E is an integer (the epoch), P is the period, and T_0 is a

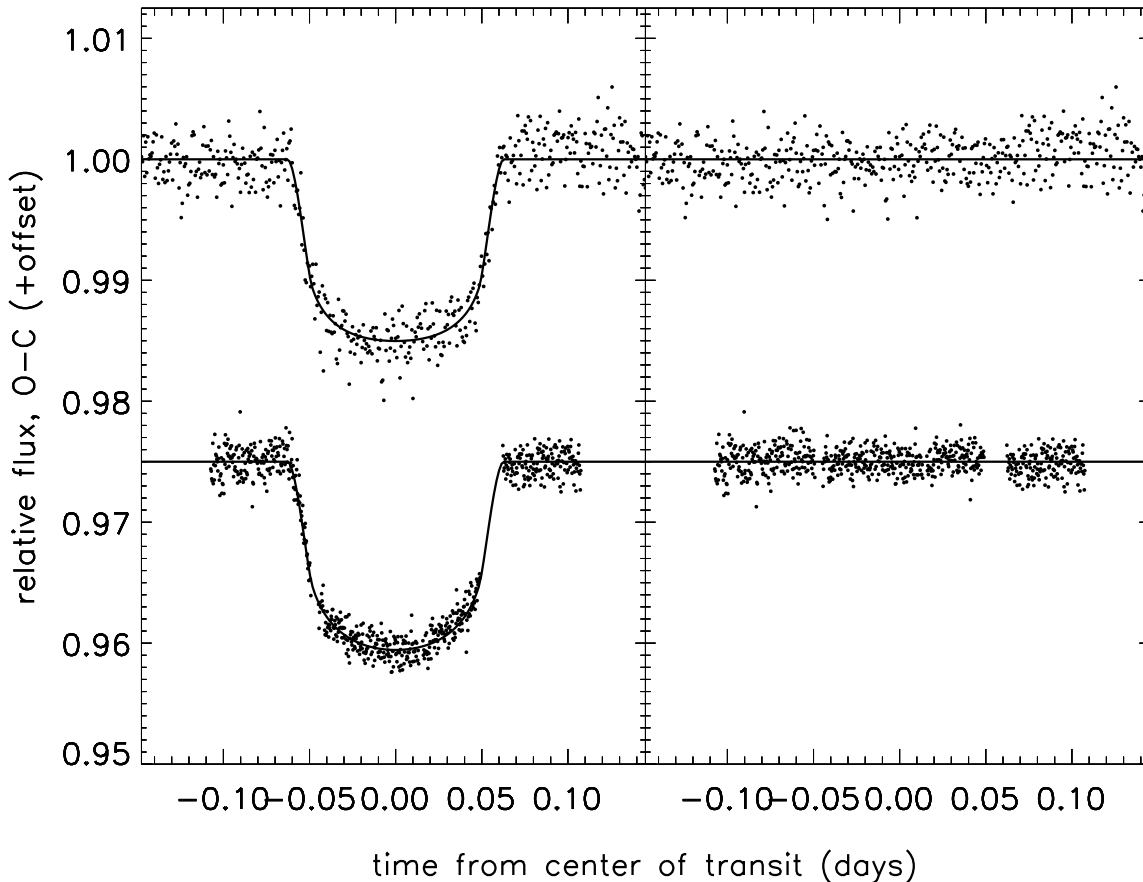


FIG. 4.— Relative photometry of WASP-12 in the z - and V -bands. The top light curve is based on z -band observations on 2009 Jan 08. See Table 1 for the cadence and rms residual of each light curve. The bottom light curve is based on V -band observations on 2009 Dec 06.

particular reference time. The best-fitting values of P and T_0 were determined by linear regression. Figures 5-7 show the residuals to the fits, and the captions specify the minimum χ^2 and the number of degrees of freedom. In no case is there clear evidence of timing anomalies. For TrES-4, there is formally only a 6% chance of obtaining such a large χ^2 with random Gaussian errors, but we do not deem this significant enough to warrant special attention.

The case of WASP-12 required somewhat special treatment because Hebb et al. (2009) did not report individual midtransit times, but rather a consensus reference time based on observations of multiple transits. We included their quoted reference time as a single data point. Campo et al. (2010) provided many transit times obtained over several years, but most of the data were from amateur observers and were not presented in detail or evaluated critically. For this reasons we did not include them; however, as a consequence, there are not many points in our fit.

The results for P and T_0 are given in Tables 5-7. They are based on a fit in which all of the uncertainties of the transit times were rescaled by a common factor to give $\chi^2/N_{\text{dof}} = 1$. Our intention is to provide conservative error estimates to allow for planning of future observations. The uncertainties on the individual transit times given in Tables 8-10 were *not* rescaled in this way, nor were the error bars that are plotted in

Figures 5-7.

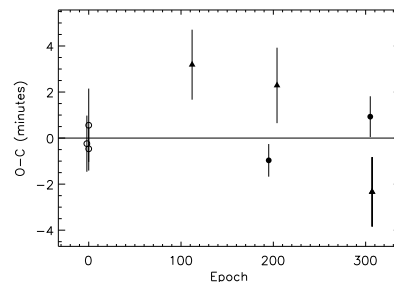


FIG. 5.— Timing residuals for TrES-4. The data presented in this paper are labeled with solid circles (complete transits) and solid triangles (partial transits). Open circles represent transits observed by Mandushev et al. (2007). The best fit gives $\chi^2 = 12.1$ with 6 degrees of freedom. The probability of obtaining a higher χ^2 with random Gaussian data points is about 6%.

5. SUMMARY AND DISCUSSION

We have presented new photometry and new analyses of the transiting exoplanets TrES-4b, HAT-P-3b, and WASP-12b. Whereas the discovery papers reporting TrES-4b and HAT-P-3b included only a few high-precision light curves, our analyses are based on 5-6 such datasets. Likewise, the WASP-12b

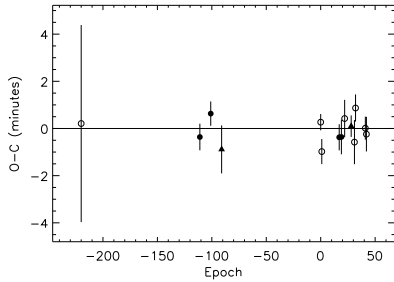


FIG. 6.— Timing residuals for HAT-P-3. The data presented in this paper are labeled with solid circles (complete transits) and solid triangles (partial transits). Open circles represent transits observed by Gibson et al. (2010); Torres et al. (2007). The best fit gives $\chi^2 = 10.4$ with 12 degrees of freedom. The probability of obtaining a higher χ^2 with random Gaussian data points is about 60%.

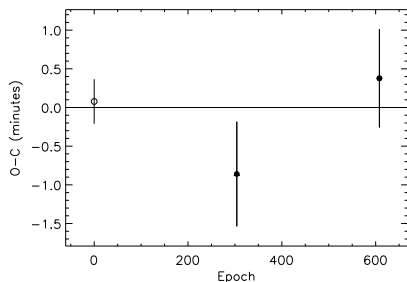


FIG. 7.— Timing residuals for WASP-12. Solid circles are complete transits that we observed, and the open circle is the reference transit time (derived from observations of multiple events) quoted by Hebb et al. (2009). The best fit gives $\chi^2 = 2.0$ with 1 degree of freedom.

discovery paper featured only one high-precision light curve, to which we have added two. We have applied consistent and conservative procedures for parameter estimation, including an accounting for uncertainties in the limb-darkening law and due to time-correlated noise, as well as linkage between the light curve parameters and stellar-evolutionary models, that were not always applied by previous authors. In the past these efforts have occasionally led to significant revisions of the planetary dimensions (see, e.g. Winn et al. 2007b, 2008).

In the present case our results are in agreement with the previously reported results. All of the TrES-4 parameters agree

to within 2σ with the results reported by Torres et al. (2008). Two of the most important parameters, the mass and radius of the planet, agree to within 1σ . Our HAT-P-3 parameters agree to within 2σ with those reported by Gibson et al. (2010), and the planetary mass and radius agree to within 1.3σ . Our WASP-12 parameters agree to within 2σ with those reported by Hebb et al. (2009), and the mass and radius of the planet agree to within 1σ .

Our transit ephemeris for TrES-4 agrees with that of Mandushev et al. (2007), and the refined orbital period is about 20 times more precise. Our ephemeris for HAT-P-3 agrees with that of Gibson et al. (2010), and is 2-3 times more precise. Our ephemeris for WASP-12 agrees with that of Hebb et al. (2009), and is of comparable precision, despite being based on only a few well-documented data points.

The reason that TrES-4, HAT-P-3, and WASP-12 are of particular interest is because their measured dimensions do not agree with standard models of gas giant planets. TrES-4 and WASP-12 are heavily bloated, with radii too large for their masses, while HAT-P-3 is too small. With reference to the tables of Fortney et al. (2007), TrES-4 and WASP-12 are incompatible with pure hydrogen-helium giant planets at the 10σ and 5σ levels, respectively. Enhancing these planets with metals to the degree of Jupiter or Saturn would only make the problem worse. HAT-P-3, in contrast, is compatible with the tabulated models if it is endowed with approximately $100 M_{\oplus}$ of heavy elements. Our results do not change these interpretations of the three systems we have studied. Rather, our results lend more confidence to the claims that the dimensions of the planets are anomalous, and merit attention by theoreticians who seek to solve the radius anomaly problem.

We thank Gerald Nordley for checking some of the entries in Tables 5-7. We gratefully acknowledge support from the NASA Origins program through award NNX09AB33G and from the Research Science Institute, a program of the Center for Excellence in Education. Some of the data presented herein were obtained with the Nordic Optical Telescope (NOT), operated on the island of La Palma jointly by Denmark, Finland, Iceland, Norway, and Sweden, in the Spanish Observatorio del Roque de los Muchachos Instituto Astrofísica de Canarias, and ALFOSC, which is owned by the Instituto Astrofísica de Andalucía (IAA) and operated at the NOT under agreement between IAA and NBIfAFG of the Astronomical Observatory of Copenhagen.

REFERENCES

- Batygin, K., & Stevenson, D. J. 2010, *ApJ*, 714, L238
 Campo, C. J., et al. 2010, *ArXiv e-prints*
 Carter, J. A., & Winn, J. N. 2009, *ApJ*, 704, 51
 Carter, J. A., Winn, J. N., Gilliland, R., & Holman, M. J. 2009, *ApJ*, 696, 241
 Charbonneau, D., Brown, T. M., Latham, D. W., & Mayor, M. 2000, *ApJ*, 529, L45
 Claret, A. 2004, *VizieR Online Data Catalog*, 342, 81001
 Droege, T. F., Richmond, M. W., Sallman, M. P., & Creager, R. P. 2006, *PASP*, 118, 1666
 Fortney, J. J., Marley, M. S., & Barnes, J. W. 2007, *ApJ*, 659, 1661
 Fortney, J. J., & Nettelmann, N. 2010, *Space Sci. Rev.*, 152, 423
 Gelman, A., & Rubin, D. B. 1992, *Statistical Science*, 7, 457
 Gibson, N. P., et al. 2010, *MNRAS*, 401, 1917
 Hebb, L., et al. 2009, *ApJ*, 693, 1920
 Henry, G. W., Marcy, G. W., Butler, R. P., & Vogt, S. S. 2000, *ApJ*, 529, L41
 Holman, M. J., et al. 2006, *ApJ*, 652, 1715
 Madhusudhan, N., et al. 2011, *Nature*, 469, 64
 Mandel, K., & Agol, E. 2002, *ApJ*, 580, L171
 Mandushev, G., et al. 2007, *ApJ*, 667, L195
 Pál, A. 2008, *MNRAS*, 390, 281
 Perna, R., Menou, K., & Rauscher, E. 2010, *ApJ*, 724, 313
 Pont, F., Zucker, S., & Queloz, D. 2006, *MNRAS*, 373, 231
 Sozzetti, A., Torres, G., Charbonneau, D., Latham, D. W., Holman, M. J., Winn, J. N., Laird, J. B., & O'Donovan, F. T. 2007, *ApJ*, 664, 1190
 Sozzetti, A., et al. 2009, *ApJ*, 691, 1145
 Torres, G., Winn, J. N., & Holman, M. J. 2008, *ApJ*, 677, 1324
 Torres, G., et al. 2007, *ApJ*, 666, L121
 Winn, J. N. 2010, *ArXiv e-prints*
 Winn, J. N., Holman, M. J., & Fuentes, C. I. 2007a, *AJ*, 133, 111
 Winn, J. N., et al. 2007b, *AJ*, 134, 1707
 —. 2008, *ApJ*, 683, 1076
 Yi, S., Demarque, P., Kim, Y., Lee, Y., Ree, C. H., Lejeune, T., & Barnes, S. 2001, *ApJS*, 136, 417

TABLE 1
JOURNAL OF OBSERVATIONS

Date [UT]	Target	Filter	Cadence Γ [min ⁻¹]	RMS σ	Red noise factor β	Notes
08 Mar 2008	HAT-P-3	<i>i</i>	1.54	0.0018	1.39	
06 Apr 2008	HAT-P-3	<i>i</i>	2.50	0.0019	1.48	
05 May 2008	HAT-P-3	<i>i</i>	2.50	0.0036	1.00	Incomplete phase coverage
18 Jan 2009	HAT-P-3	<i>z</i>	0.58	0.55	–	Bad weather ^a
14 Mar 2009	HAT-P-3	<i>z</i>	0.81	0.0010	1.31	
20 Mar 2009	HAT-P-3	<i>z</i>	0.67	0.0014	1.24	Incomplete phase coverage
15 Apr 2009	HAT-P-3	<i>z</i>	0.81	0.0012	1.05	
18 Apr 2009	HAT-P-3	<i>z</i>	0.81	0.0013	–	Bad weather ^a
30 Jan 2010	HAT-P-3	<i>z</i>	0.58	0.0029	–	Very incomplete phase coverage ^a
10 Jun 2008	TrES-4	<i>i</i>	0.81	0.0013	1.06	Incomplete phase coverage
01 Apr 2009	TrES-4	<i>i</i>	0.81	0.0012	1.00	
03 May 2009	TrES-4	<i>i</i>	0.67	0.0009	1.42	Incomplete phase coverage
28 May 2009	TrES-4	<i>i</i>	0.71	0.0011	–	Very incomplete phase coverage ^a
06 Jul 2009	TrES-4	<i>i</i>	0.67	0.0013	–	Very incomplete phase coverage ^a
27 Apr 2010	TrES-4	<i>i</i>	0.45	0.0016	1.00	
04 May 2010	TrES-4	<i>i</i>	0.67	0.0012	1.15	Partial transit only
16 Jun 2010	TrES-4	<i>i</i>	0.81	0.0011	–	Very incomplete phase coverage ^a
18 Dec 2008	WASP-12	<i>z</i>	0.80	0.0020	–	Bad weather ^a
08 Jan 2009	WASP-12	<i>z</i>	1.50	0.0018	1.48	
18 Jan 2009	WASP-12	<i>z</i>	0.67	0.0019	–	Bad weather ^a
19 Jan 2009	WASP-12	<i>z</i>	1.00	0.0011	–	Bad weather ^a
07 Mar 2009	WASP-12	<i>z</i>	0.80	0.0012	–	Bad weather ^a
06 Dec 2009	WASP-12	<i>V</i>	6.33	0.0011	1.57	Observed using the NOT
12 Jan 2010	WASP-12	<i>z</i>	1.00	0.0020	–	Bad weather ^a
24 Jan 2010	WASP-12	<i>z</i>	0.50	0.0031	–	Bad weather ^a
25 Jan 2010	WASP-12	<i>z</i>	0.50	0.0023	–	Bad weather ^a
18 Feb 2010	WASP-12	<i>z</i>	0.40	0.0018	–	Bad weather ^a
01 Mar 2010	WASP-12	<i>z</i>	0.80	0.0049	–	Bad weather ^a

^a Data not used in calculations.

TABLE 2
PHOTOMETRY OF TRÉS-4 (EXCERPT)

Filter	HJD _{UTC}	Relative flux	Airmass
<i>i</i>	2454628.84123771	1.00133657	1.0055
<i>i</i>	2454628.84212893	0.99907639	1.0058
<i>i</i>	2454628.84384188	0.99966428	1.0062

NOTE. — The time-stamp represents the UT-based Heliocentric Julian Date at midexposure. We intend for the rest of this table to be available online.

TABLE 3
PHOTOMETRY OF HAT-P-3 (EXCERPT)

Filter	HJD _{UTC}	Relative flux	Airmass
<i>i</i>	2454534.74665524	1.00252886	1.5209
<i>i</i>	2454534.74709502	0.99836326	1.5175
<i>i</i>	2454534.74755801	1.00316729	1.5142

NOTE. — The time-stamp represents the UT-based Heliocentric Julian Date at midexposure. We intend for the rest of this table to be available online.

TABLE 4
PHOTOMETRY OF WASP-12 (EXCERPT)

Filter	HJD _{UTC}	Relative flux	Airmass
<i>z</i>	2454840.62025635	1.00042427	1.5419
<i>z</i>	2454840.62085820	1.00001333	1.5362
<i>z</i>	2454840.62148318	1.00215610	1.5304

NOTE. — The time-stamp represents the UT-based Heliocentric Julian Date at midexposure. We intend for the rest of this table to be available online.

TABLE 5
SYSTEM PARAMETERS FOR TRES-4

Parameter	Symbol	Value	68.3% Conf. Limits	Comment ^a
<i>Transit parameters:</i>				
Orbital period [d]	P	3.5539268	± 0.000032	LC
Midtransit time [HJD _{UTC}]	T_0	2454230.90524	± 0.00062	LC
Planet-to-star radius ratio	R_p/R_*	0.09745	± 0.00076	LC
Orbital inclination [deg]	i	82.81	± 0.37	LC
Scaled semimajor axis	a/R_*	6.08	± 0.16	LC
Transit impact parameter	b	0.761	± 0.018	LC
Transit duration [hr]		3.567	± 0.037	LC
Transit ingress or egress duration [hr]		0.692	± 0.047	LC
<i>Other orbital parameters:</i>				
Orbital eccentricity	e	0		Adopted
Velocity semiamplitude [m s ⁻¹]	K	97.4	± 7.2	K
Planet-to-star mass ratio	M_p/M_*	0.000631	± 0.000047	LC + M + T + Y ² + K
Semimajor axis [AU]	a	0.05084	± 0.00050	LC + M + T + Y ²
<i>Stellar parameters:</i>				
Mass [M_\odot]	M_*	1.388	± 0.042	LC + M + T + Y ²
Radius [R_\odot]	R_*	1.798	± 0.052	LC + M + T + Y ²
Mean density [g cm ⁻³]	ρ_*	0.337	± 0.027	LC
Effective temperature [K]	T_{eff}	6200	± 75	T
Projected rotation rate [km s ⁻¹]	$v \sin i_*$	9.5	± 1.0	PRR
Surface gravity [cgs]	$\log g_*$	4.071	± 0.024	LC + M + T + Y ²
Metallicity [dex]	[Fe/H]	+0.14	± 0.09	M
Luminosity [L_\odot]	L_*	4.25	± 0.41	LC + M + T + Y ²
Visual Magnitude [mag]	M_V	3.19	± 0.12	LC + M + T + Y ²
Apparent Magnitude [mag]	m_V	11.592	± 0.004	m_V
Age [Gyr]		2.9	± 0.3	LC + M + T + Y ²
Distance [pc]		479	± 26	LC + M + T + Y ² + m_V
<i>Planetary parameters:</i>				
Mass [M_{Jup}]	M_p	0.917	± 0.070	LC + M + T + Y ² + K
Radius [R_{Jup}]	R_p	1.706	± 0.056	LC + M + T + Y ²
Surface gravity [cgs]	$\log g_p$	2.893	± 0.042	LC + K
Mean density [g cm ⁻³]	ρ_p	0.229	± 0.027	LC + M + T + Y ²

^a The type of data used to calculate the given quantity. LC denotes light curve data. M and T denote metallicity and temperature respectively and were taken from Sozzetti et al. (2009). K, PRR, and m_V denote velocity semiamplitude, projected rotation rate, and apparent magnitude respectively and were taken from Mandushev et al. (2007). Y² denotes the Yonsei-Yale isochrones (Yi et al. 2001)

TABLE 6
SYSTEM PARAMETERS FOR HAT-P-3

Parameter	Symbol	Value	68.3% Conf. Limits	Comment ^a
<i>Transit parameters:</i>				
Orbital period [d]	P	2.8997360	± 0.0000020	LC
Midtransit time [HJD _{UTC}]	T_0	2454856.70118	± 0.00010	LC
Planet-to-star radius ratio	R_p/R_*	0.1063	± 0.0020	LC
Orbital inclination [deg]	i	87.07	± 0.55	LC
Scaled semimajor axis	a/R_*	10.39	± 0.49	LC
Transit impact parameter	b	0.530	± 0.075	LC
Transit duration [hr]		2.075	± 0.022	LC
Transit ingress or egress duration [hr]		0.270	± 0.033	LC
<i>Other orbital parameters:</i>				
Orbital eccentricity	e	0		Adopted
Velocity semiamplitude [m s ⁻¹]	K	89.1	± 2.0	K
Planet-to-star mass ratio	M_p/M_*	0.000615	± 0.000015	LC + M + T + Y ² + K
Semimajor axis [AU]	a	0.03866	± 0.00041	LC + M + T + Y ²
<i>Stellar parameters:</i>				
Mass [M_\odot]	M_*	0.917	± 0.030	LC + M + T + Y ²
Radius [R_\odot]	R_*	0.799	± 0.039	LC + M + T + Y ²
Mean density [g cm ⁻³]	ρ_*	2.53	± 0.36	LC
Effective temperature [K]	T_{eff}	5185	± 80	T
Projected rotation rate [km s ⁻¹]	$v \sin i_*$	0.5	± 0.5	PRR
Surface gravity [cgs]	$\log g_*$	4.594	± 0.041	LC + M + T + Y ²
Metallicity [dex]	[Fe/H]	+0.27	± 0.08	M
Luminosity [L_\odot]	L_*	0.435	± 0.053	LC + M + T + Y ²
Visual Magnitude [mag]	M_V	5.87	± 0.15	LC + M + T + Y ²
Apparent Magnitude [mag]	m_V	11.577	± 0.067	m_V
Age [Gyr]		1.6	-1.3,+2.9	LC + M + T + Y ²
Distance [pc]		138	± 10	LC + M + T + Y ² + m_V
<i>Planetary parameters:</i>				
Mass [M_{Jup}]	M_p	0.591	± 0.018	LC + M + T + Y ² + K
Radius [R_{Jup}]	R_p	0.827	± 0.055	LC + M + T + Y ²
Surface gravity [cgs]	$\log g_p$	3.330	± 0.058	LC + K
Mean density [g cm ⁻³]	ρ_p	1.29	± 0.25	LC + M + T + Y ²

^a The type of data used to calculate the given quantity. LC denotes light curve data, K, M, T, and PRR denote velocity semiamplitude, metallicity, temperature, and projected rotation rate respectively and were taken from Torres et al. (2007). The uncertainties in M and T were adjusted as suggested by Torres et al. (2008). m_V denotes apparent magnitude and was taken from Droege et al. (2006). Y² denotes the Yonsei-Yale isochrones (Yi et al. 2001).

TABLE 7
SYSTEM PARAMETERS FOR WASP-12

Parameter	Symbol	Value	68.3% Conf. Limits	Comment ^a
<i>Transit parameters:</i>				
Orbital period [d]	P	1.0914222	± 0.0000011	LC
Midtransit time [HJD _{UTC}]	T_0	2454508.97605	± 0.00028	LC
Planet-to-star radius ratio	R_p/R_*	0.1119	± 0.0020	LC
Orbital inclination [deg]	i	86.0	± 3.0	LC
Scaled semimajor axis	a/R_*	3.097	± 0.082	LC
Transit impact parameter	b	0.22	± 0.15	LC
Transit duration [hr]		3.001	± 0.037	LC
Transit ingress or egress duration [hr]		0.324	± 0.020	LC
<i>Other orbital parameters:</i>				
Orbital eccentricity	e	0		Adopted
Velocity semiamplitude [m s ⁻¹]	K	226	± 4	K
Planet-to-star mass ratio	M_p/M_*	0.000993	± 0.000038	LC + M + T + Y ² + K
Semimajor axis [AU]	a	0.02293	± 0.00078	LC + M + T + Y ²
<i>Stellar parameters:</i>				
Mass [M_\odot]	M_*	1.35	± 0.14	LC + M + T + Y ²
Radius [R_\odot]	R_*	1.599	± 0.071	LC + M + T + Y ²
Mean density [g cm ⁻³]	ρ_*	0.472	± 0.038	LC
Effective temperature [K]	T_{eff}	6300	± 150	T
Projected rotation rate [km s ⁻¹]	$v \sin i_*$	< 2.2	± 1.5	PRR
Surface gravity [cgs]	$\log g_*$	4.162	± 0.029	LC + M + T + Y ²
Metallicity [dex]	[Fe/H]	0.30	± 0.10	M
Luminosity [L_\odot]	L_*	3.0	± 1.2	LC + M + T + Y ²
Visual Magnitude [mag]	M_V	3.54	± 0.38	LC + M + T + Y ²
Apparent Magnitude [mag]	m_V	11.69	± 0.08	m_V
Age [Gyr]		1.7	± 0.8	LC + M + T + Y ²
Distance [pc]		427	± 90	LC + M + T + Y ² + m_V
<i>Planetary parameters:</i>				
Mass [M_{Jup}]	M_p	1.404	± 0.099	LC + M + T + Y ² + K
Radius [R_{Jup}]	R_p	1.736	± 0.092	LC + M + T + Y ²
Surface gravity [cgs]	$\log g_p$	3.066	± 0.031	LC + K
Mean density [g cm ⁻³]	ρ_p	0.337	± 0.039	LC + M + T + Y ²

^a The type of data used to calculate the given quantity. LC denotes light curve data. K, M, T, PRR, and m_V denote velocity semiamplitude, metallicity, temperature, projected rotation rate and apparent magnitude respectively, and were taken from Hebb et al. (2009) (the uncertainties were symmetrized). Y² denotes the Yonsei-Yale isochrones (Yi et al. 2001).

TABLE 8
MIDTRANSIT TIMES FOR TRES-4

Epoch	Midtransit Time [HJD]	Uncertainty	Filter	Source
-2	2454223.797215	0.000847	z	Sozzetti et al. (2009) ^a
0	2454230.904913	0.000656	z	Sozzetti et al. (2009) ^a
0	2454230.905624	0.001106	B	Sozzetti et al. (2009) ^a
112	2454628.947249	0.001056	i	This paper ^b
195	2454923.920285	0.000492	i	This paper
204	2454955.907886	0.001138	i	This paper ^b
305	2455314.853547	0.000616	i	This paper
307	2455321.959132	0.001049	i	This paper ^b

^a Transits were observed by Mandushev et al. (2007) but re-analyzed by Sozzetti et al. (2009)

^b Partial transit observed

TABLE 9
MIDTRANSIT TIMES FOR HAT-P-3

Epoch	Midtransit Time [HJD]	Uncertainty	Filter	Source
-220	2454218.759400	0.002900	i	Torres et al. (2007)
-111	2454534.830232	0.000391	i	This paper
-101	2454563.828281	0.000358	i	This paper
-91	2454592.824589	0.000707	i	This paper ^a
0	2454856.701370	0.000240	- ^b	Gibson et al. (2010)
1	2454859.600240	0.000370	- ^b	Gibson et al. (2010)
17	2454905.996437	0.000385	z	This paper
19	2454911.795918	0.000510	z	This paper ^a
22	2454920.495670	0.000550	- ^b	Gibson et al. (2010)
28	2454937.893861	0.000317	z	This paper
31	2454946.592600	0.000650	- ^b	Gibson et al. (2010)
32	2454949.493340	0.000400	- ^b	Gibson et al. (2010)
41	2454975.590370	0.000340	- ^b	Gibson et al. (2010)
42	2454978.489930	0.000510	- ^b	Gibson et al. (2010)

^a Partial transit observed

^b A single wideband filter ($\approx 500-700\text{nm}$) was used.

TABLE 10
MIDTRANSIT TIMES FOR WASP-12

Epoch	Midtransit Time [HJD]	Uncertainty	Filter	Source
0	2454508.97610	0.00020	...	Hebb et al. (2009) ^a
304	2454840.76781	0.00047	V	This paper
608	2455172.56103	0.00044	V	This paper

^a This data point actually represents a consensus value derived from observations of several transits.